Research Square

Preprints are preliminary reports that have not undergone peer review.
They should not be considered conclusive, used to inform clinical practice,
or referenced by the media as validated information.

Deformation Mechanism-Based Analysis of Blank Holder Force Paths in Hydromechanical Deep Drawing of Parabolic Cups

Thanasan Intarakumthornchai

King Mongkut's University of Technology North Bangkok

Yingyot Aue-u-lan

yingyot.a@tggs.kmutnb.ac.th

King Mongkut's University of Technology North Bangkok https://orcid.org/0000-0002-2925-4974

Research Article

Keywords: Hydromechanical deep drawing (HMD), Parabolic cup, Stage-based mechanics, Forming limit diagram (FLD), Bi-linear blank holder force (BHF)

Posted Date: November 10th, 2026

DOI: https://doi.org/10.21203/rs.3.rs-11396091/v1

License: This work is licensed under a Creative Commons Attribution 4.0 International License.
Read Full License

Deformation Mechanism-Based Analysis of Blank Holder Force Paths in Hydromechanical Deep Drawing of Parabolic Cups

Thanasan Intarakumthornchai[1], Yingyot Aue-u-lan[2*]

[1] Department of Industrial Engineering, Faculty of Engineering, King Mongkut's University of Technology North Bangkok, Bangkok, Thailand

[2] Department of Mechanical and Process Engineering, Materials and Production Engineering Program, The Sirindhorn International Thai-German Graduate School of Engineering, King Mongkut's University of Technology North Bangkok, Bangkok, Thailand

[*] **Corresponding author:** Yingyot Aue-u-lan (e-mail: yingyot.a@tggs.kmutnb.ac.th)

Abstract In hydromechanical deep drawing (HMD) of parabolic cups made of SPCC cold-rolled low-carbon steel grade JIS G 3141, localized thinning at the acute apex is a persistent failure that conventional "black-box" optimization methods cannot physically explain. This study develops a mechanism-informed methodology that integrates physical experiments with a validated finite element (FE) model. Interrupted drawing experiments then divided the HMD process into four transient stages (pre-bulge, thin-out, draw-in, and re-strike) and identified the thin-out stage, at a punch stroke of 73 mm, as the critical failure window. An LS-DYNA FE model was calibrated with these measurements, and forming limit diagram (FLD) analysis was used to evaluate the strain paths. A linear blank holder force (BHF) profile that keeps the force low during the thin-out stage shifted the average strain state from a uniaxial tensile mode (strain ratio $\beta = -0.50$) toward a drawing-dominated mode ($\beta = -0.69$), increasing material draw-in by 59.1% and reducing the maximum thinning from 30 to 25%. To avoid the flange wrinkling caused by an excessive BHF reduction, a bi-linear BHF profile was proposed to lower the force during the thin-out stage and increase it during the draw-in and re-strike stages; FE simulation predicts a further reduction in maximum thinning to 23.74% without flange wrinkling. As the four-stage deformation sequence and the thin-out-driven failure mechanism arise from the

part's acute curvature, this procedure of stage identification, FLD-based diagnosis, and stage-dependent BHF design may be transferable to other severely curved axisymmetric HMD components.

Keywords Hydromechanical deep drawing (HMD) · Parabolic cup · Stage-based mechanics · Forming limit diagram (FLD) · Bi-linear blank holder force (BHF)

1 Introduction

Parabolic cups are essential components in light reflectors for high-precision and advanced optical systems. However, the cups have specific geometries characterized by severe tapers and an acute apex, which lead to significant formability challenges during conventional deep drawing processes. Due to the minimal cross-sectional area at the punch head, the drawing load induces a high risk of localized fracture even at modest drawing ratios. Furthermore, the extensive unsupported zone between the die and punch often triggers sidewall wrinkling caused by circumferential compressive stresses. Historically, overcoming these defects necessitated at least six individual forming stages, as illustrated in Fig. 1 [1].

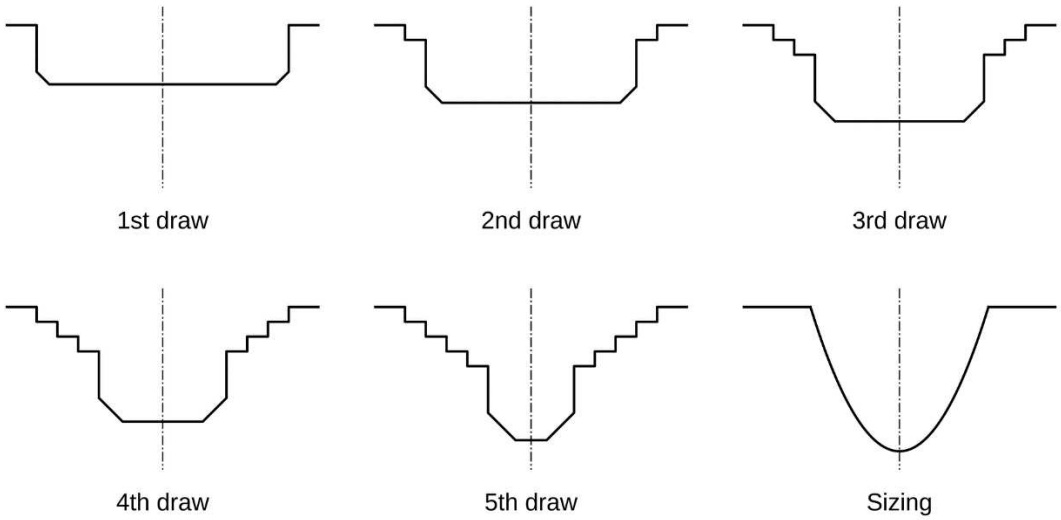


Fig. 1 Schematic of the conventional multi-stage deep drawing sequence for a parabolic cup (redrawn based on [1])

Hydromechanical deep drawing (HMD) was developed as an advanced alternative for fabricating complicated curvilinear components, where fluid pressure is used to offer hydrostatic support and enhance the overall distribution of strain [1–3]. However, the extreme geometry of the parabolic apex remains highly susceptible to severe local thinning and wrinkling [4]. Although there has been extensive work in optimizing loading paths, most studies are limited to purely numerical or stochastic optimization frameworks.

To determine optimal process parameters, researchers have employed various analytical and numerical techniques. Analytical models and empirical foundations provided by Koç [5] have served as essential starting points for process design. The optimal loading paths were further investigated based on FEA-based optimizations by Choi et al. [6] and Öztürk et al. [7]. Later, Intarakumthornchai et al. [8] reported the optimization of process parameters using response surface methodology (RSM) to optimize HMD parameters. Other studies examined how pre-bulging before punch contact affects the subsequent deformation in HMD [9] and optimized the die design parameters using FE simulation [10]. Lang et al. [9] showed that the pre-bulging significantly affects the initial and middle forming stages, but it does not influence the final forming stage. Liu et al. [4] extended their study further on the effect of pre-bulging on the wrinkle of curved-surface parts. These findings indicate that the effect of a process variable is highly dependent on the stage of the stroke at which it acts, which suggests that the HMD stroke should be treated at each continuous sequential stage rather than as a single event. The abovementioned studies determined the process parameters acting on each stroke as a whole, but they did not identify each stage experimentally or apply them to set the loading path.

Variable blank holder force (VBHF) control, in which the BHF changes with the punch stroke, has long been recognized as an effective means of widening the process window between wrinkling and tearing [11]. VBHF trajectories have been determined by adaptive FE simulation with wrinkling and thinning criteria [12], by optimization strategies that combine FE simulation

with formability constraints [13], and by fuzzy control integrated into adaptive FE analysis of HMD [7]. In sheet hydroforming, VBHF has also been implemented experimentally to improve the drawability of square cups [14]. In these studies, however, the BHF trajectory is typically obtained as the output of a control or optimization loop, and the transient deformation stages that make a particular trajectory effective are rarely identified experimentally.

Recently, HMD has been investigated for lightweight and composite materials such as magnesium alloys and laminated sheets [15–19]. These studies yield valuable data about the behavior of the material using stochastic optimization or arbitrary time-stepping for BHF control [20]. Experimental evidence to characterize the transient mechanical changes during forming stages is lacking, although numerical verifications have been done [21]. This is important to prevent localized thinning in acute geometries such as parabolic cups.

In a previous study by Intarakumthornchai et al. [8], RSM was employed to optimize the constant process parameters for HMD of parabolic cups. While RSM provided a statistical optimum for a given range, it functioned as a "black-box" approach that could not account for transient mechanical changes occurring at different punch strokes. Furthermore, reliance on a constant blank holder force (BHF) in that work limited the ability to prevent thinning at the acute apex without risking wrinkles. Crucially, empirical evidence validating the dynamic, stage-by-stage mechanical evolution of acute geometries during HMD remains largely absent from the literature.

To overcome the limitations of these statistically based models [8], the present study shifts toward a fully mechanism-informed approach. By implementing systematic interrupted drawing experiments, this work physically deconstructs the parabolic HMD process within a single forming stroke into four distinct transient stages, in contrast to the multiple separate tooling operations historically required. This stage-based mechanical characterization enables a targeted approach, allowing for the design of a bi-linear BHF profile. The novelty of this

work therefore does not lie in reducing the BHF itself, which is well established in VBHF studies [11–14], but in deriving the timing and breakpoints of the BHF path from experimentally identified deformation stages, so that each segment of the profile has a physical justification. This shift from a single constant optimum for all phases to stage-dependent dynamic control is a key step toward improving both the resistance to thinning and the structural integrity against wrinkling.

2 Materials and Methods

2.1 Material characterization

The material used in this research was SPCC (JIS G 3141) cold-rolled low-carbon steel with a 1.0 mm nominal thickness. Uniaxial tensile tests were conducted according to ASTM E8 on a 1-ton Instron universal testing machine equipped with a video extensometer, using 30 specimens cut at 0°, 45°, and 90° to the rolling direction (90 specimens in total). The mechanical properties, including yield strength (σ_y), ultimate tensile strength (UTS), strain hardening exponent (n), and plastic anisotropy ratio (r), were determined. The uniaxial tensile tests gave a yield strength of 267 MPa and an ultimate tensile strength of 471 MPa. The mean anisotropy ratios were $r_0 = 1.816$, $r_{45} = 1.228$, and $r_{90} = 2.106$, giving a normal anisotropy of $r_m = (r_0 + 2r_{45} + r_{90})/4 \approx 1.6$. The material exhibits pronounced strain hardening and normal anisotropy, both of which strongly influence the drawability of a parabolic geometry.

Even though the uniaxial tensile tests provided flow stress data only up to a true strain of approximately 0.3 ($K = 512.3$ MPa, $n = 0.159$), the hardening parameters used in the simulation were determined by hydraulic bulge tests (HBT), which extend the flow curve to effective strains of 0.7–0.8. The HBT die had an opening diameter of 100 mm and a die radius of 5 mm, and the tests were performed on a 200-ton hydraulic press equipped with a pressure intensifier. Since the dome thickness and radius could not be measured during forming, the tests were interrupted at seven dome heights (5–35 mm, monitored by an LVDT), with five specimens

per height, and the dome geometry and thickness were measured after each interruption. The biaxial stress obtained from the membrane equation was converted into an effective stress corrected for normal anisotropy using r_m. Power-law fits to the four complete flow curves gave $K = 659.5 \pm 1.35$ MPa and $n = 0.294 \pm 0.010$ (mean ± standard deviation), which were used in the simulation. Fig. 2 shows the pooled effective stress–strain data of all HBT specimens; a single power-law fit to the pooled data gives almost identical parameters ($K = 659.5$ MPa, $n = 0.296$). The averaged mechanical properties used for the simulation are summarized in Table 1.

Table 1 Blank geometry and material properties of the SPCC steel sheet; K and n are averaged from the four HBT flow stress curves, and r values are averaged from 30 tensile specimens per direction (HBT: hydraulic bulge test)

Parameter	**Value**
Blank diameter	320 mm
Blank thickness (t_0)	1.0 mm
Part depth	105 mm
Young's modulus (E)	207 GPa
Poisson's ratio (v)	0.28
Yield strength (σ_y)	267 MPa (tensile test)
Ultimate tensile strength (UTS)	471 MPa (tensile test)
Strain hardening exponent (n)	0.294 ± 0.010 (HBT, mean ± SD)
Strength coefficient (K)	659.5 ± 1.35 MPa (HBT, mean ± SD)
Anisotropy ratio (r_0)	1.816 (tensile test, average)
Anisotropy ratio (r_{45})	1.228 (tensile test, average)
Anisotropy ratio (r_{90})	2.106 (tensile test, average)

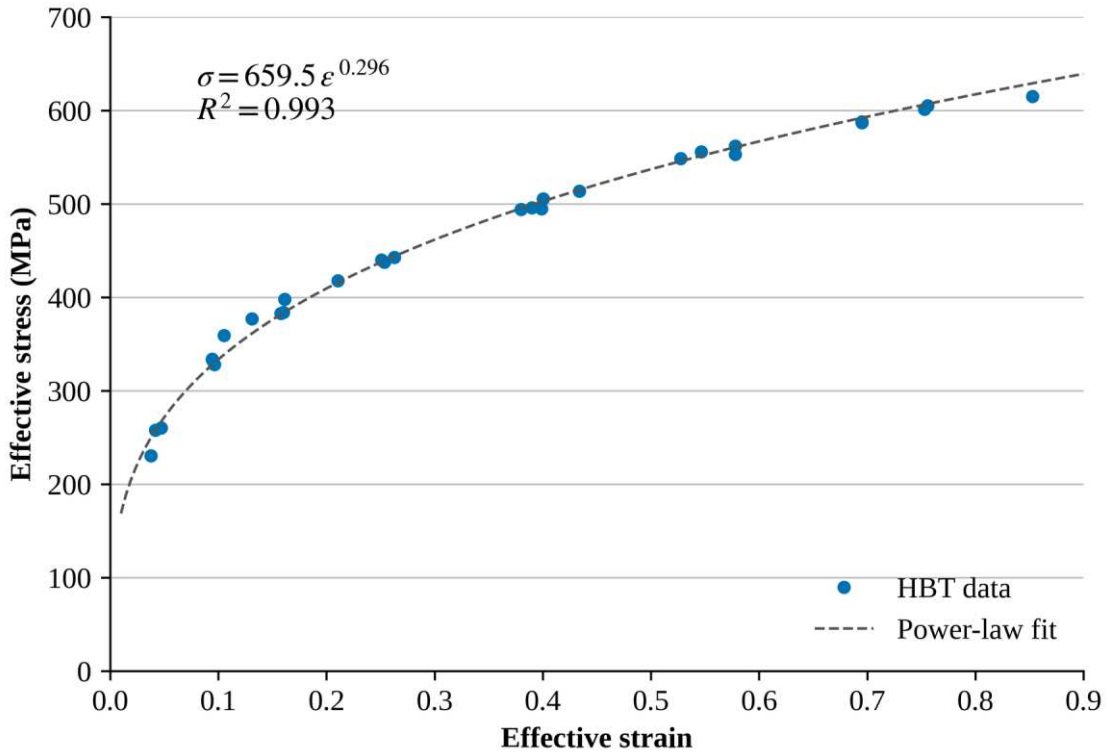


Fig. 2 Effective stress–strain data of the SPCC steel sheet obtained from all hydraulic bulge test (HBT) specimens, with the fitted power-law hardening curve

2.2 Empirical analytical foundation

The initial process window was established using the empirical equations of Koç [5]. These equations were employed to determine the theoretical minimum forming pressure ($p_{\min}$, Eq. (1)) and the minimum blank holder force (Min F_{BH}, Eq. (2)) required to suppress wrinkling while avoiding premature fracture:

$$p_{\min} = \frac{\sigma_{\mathrm{yield}} \times t_0}{r_{\min}} \tag{1}$$

where $p_{\min}$ is the minimum pressure to begin forming (MPa), σ_{yield} is the yield strength of the blank material (MPa), t_0 is the initial thickness of the blank (mm), and $r_{\min}$ is the minimum radius of the part (mm).

$$\mathrm{Min}\ F_{\mathrm{BH}} = p_{\mathrm{n}} \frac{\pi}{4} (D_0^2 - D_{\mathrm{s}}^2) + F_{\mathrm{BH/pressure}} + F_{\mathrm{BH/bulge}} \tag{2}$$

where p_n is the blank holder pressure, D_0 is the outgoing blank diameter, D_s is the sealing diameter, $F_{BH/pressure}$ is the vertical force from the pressure acting on the blank holder, and $F_{BH/bulge}$ is the bulge force acting on the blank holder. Two concepts are important:

- The pressure profile is the initial pressure path chosen to provide sufficient hydrostatic support against the compressive circumferential stresses.
- The BHF calculation yields the boundary conditions for the blank holder. These were derived from the plastic anisotropy (r-value) and geometry to maintain the seal and control material flow.

The values used for the first experimental trials are listed in Table 2.

Table 2 Pressure and BHF calculation results

Parameter	Value	Unit
Thickness (t_0)	1.00	mm
Minimum radius (r_{min})	12.00	mm
Yield strength (σ_{yield})	267.00	MPa
Ultimate tensile strength (UTS)	471.00	MPa
Minimum pressure (p_{min})	22.25	MPa
Average pressure (p_{avg})	30.75	MPa
Maximum pressure (p_{max})	39.25	MPa
Blank diameter (D_0)	320.00	mm
Punch diameter (D_{punch})	179.00	mm
Minimum BHF (Min F_{BH})	203.60	kN
Maximum BHF (Max F_{BH})	951.36	kN
Operating BHF applied	800.00	kN

2.3 Experimental procedure: interrupted drawing

A specialized HMD press was used for the physical trials. Interrupted drawing experiments were performed to deconstruct the forming mechanics. The process was stopped at specific punch heights (−20, 0, 27, 53, 79, and 105 mm). Punch height is measured from the die face, so that 0 mm corresponds to the first contact between the punch nose and the pre-bulged blank.

159 The BHF profiles represented in Sects. 3.2 and 3.4 are plotted against the press stroke s, which
160 starts at a punch height of −20 mm ($s = h + 20$ mm); the interrupted heights therefore
161 correspond to strokes of 0, 20, 47, 73, 99, and 125 mm, respectively (Table 3). Fig. 3a shows
162 the die setup, and Fig. 3b shows the experimental parts from each step. The sheet was covered
163 with a thin polyethylene (PE) film to reduce friction. Each experiment was performed in
164 triplicate.

165 • **Measurements:** Each interrupted specimen was sectioned along its centerline, and the
166 thickness was measured along the curvilinear profile and converted into thickness
167 reduction (thinning) relative to the initial thickness. The change in the peripheral
168 boundary of the flange (draw-in amount) was also measured.

169 • **Mechanism identification:** The correlation between punch stroke and material
170 response (thinning rate and draw-in speed) was used to define the boundaries of the
171 forming stages.

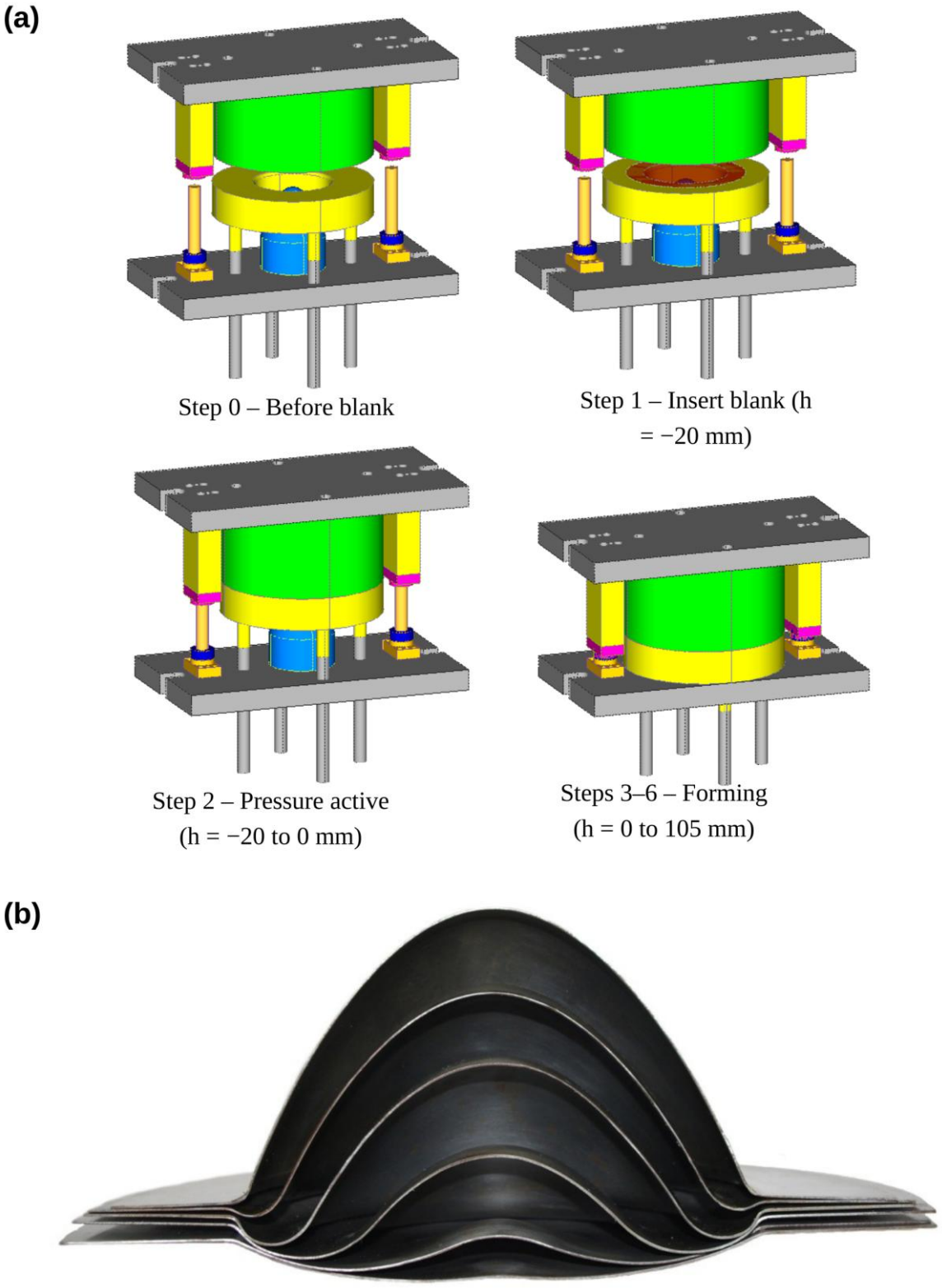


Fig. 3 Experimental setup and physical specimens: (a) hydromechanical deep drawing die configuration at each process step; (b) interrupted specimens formed to different punch heights

2.4 Finite element formulation

A finite element model was developed in LS-DYNA using Belytschko-Tsay shell elements. A quarter model (Fig. 4) was employed to exploit symmetry and minimize calculation time. The structured mesh of the blank comprised 8,000 quadrilateral elements with 8,161 nodes, giving an average in-plane element size of approximately 1.6 mm, which is small compared with the minimum part radius of 12 mm. A separate mesh-convergence study was not performed; instead, a fine mesh was adopted, and the close agreement between the predicted and measured maximum thinning for both BHF profiles (30.33% vs. 30% and 24.25% vs. 25%; Sect. 3.2) indicates that the mesh resolution is adequate for the thinning predictions reported here. A Coulomb friction model was applied at the tool-blank interfaces with a friction coefficient of $\mu = 0.05$ for the punch, blank holder, and die regions; this low value represents the lubricated condition provided by the polyethylene film covering the sheet (Sect. 2.3). The Barlat-Lian's three-parameter yield criterion was used for the blank material, and isotropic hardening was described by a power law, $\sigma = K\varepsilon^n$, with the strength coefficient K and strain hardening exponent n listed in Table 1. The fluid pressure in the die cavity was applied as a pressure load on the blank surface according to the prescribed pressure path. No mass scaling was used in the explicit analysis. The FE model was calibrated using the material properties in Table 1 and validated against the initial interrupted drawing experiments. This FE model was then employed to test the hypothesis that a linear BHF profile designed to minimize force during the identified critical thin-out stage would shift the deformation mode and improve overall part quality.

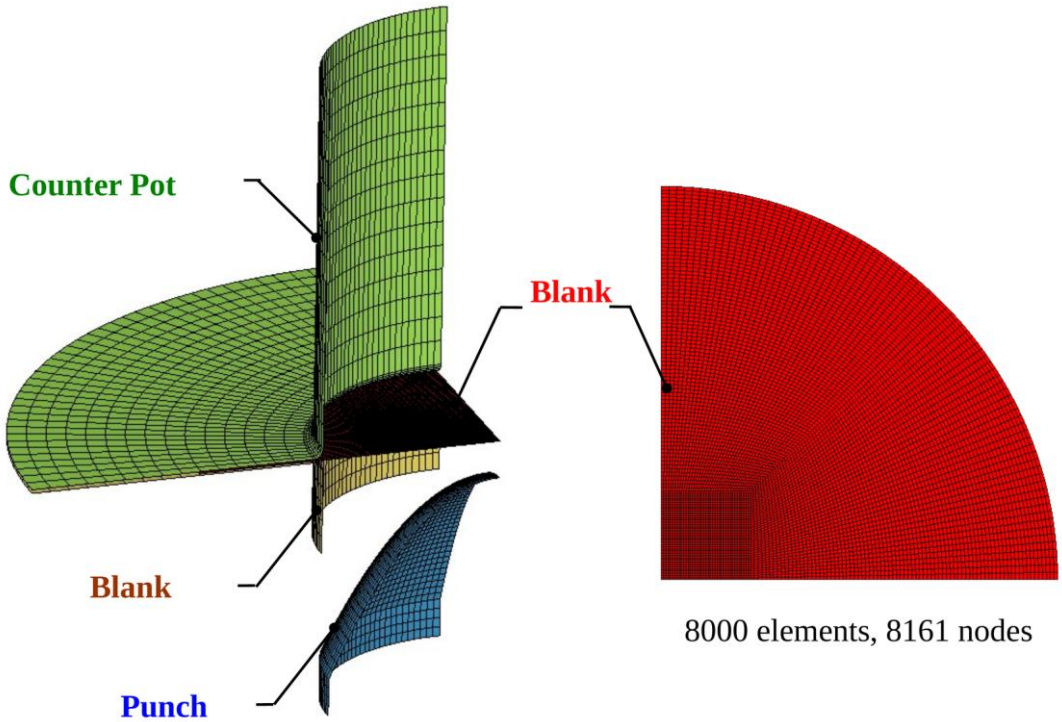


Fig. 4 Finite element quarter model of the blank and tool components

3 Results and Discussion

3.1 Experimental characterization of forming stages

Interrupted forming experiments provided critical insights into the transient mechanics of the HMD process; the tool and die setting is shown in Fig. 3a. The geometric evolution of a parabolic cup throughout the forming stroke is visually presented by the samples shown in Fig. 3b. A blank is first bulged downward into a dome and then formed upward by the punch until the final stroke. Analysis of the thickness distribution (Fig. 5) and the flange draw-in (Fig. 6) across the six forming steps reveals a consistent sequence of deformations, allowing the process to be characterized into four distinct stages. This stage-based model is conceptually summarized in Fig. 7 and is critical to understanding the root causes of defects and to targeted process control.

Stage 1: Pre-bulge. Before the punch engages, the fluid pressure deforms the blank into an initial dome. Pre-bulging is a known feature of HMD, and its influence on thickness

distribution and wrinkling has been investigated previously [4, 9]; in the present process, the pre-bulged dome forms the initial condition for the subsequent thin-out stage.

Stage 2: Thin-out. Physical measurements of the specimens revealed that thinning accelerated dramatically on initial punch contact. The punch nose contacts the pre-bulged dome and moves in the opposite direction of the bulge. This action reverses and stretches the already thinned material, causing a rapid acceleration of thinning, as can be seen from the jump from 13% to 27% maximum thinning between Steps 2 and 3 (Fig. 5). The thinnest point also shifts from the apex to a region 10 mm along the vertical direction below it, corresponding to the punch nose radius. In this stage, the sheet is subjected to severe biaxial tension. The high, constant BHF restricts material flow from the flange, forcing deformation to be accommodated almost entirely by thinning of the unsupported wall.

Stage 3: Draw-in. In Steps 4–6, the metal in the flange starts to flow inward, which is corroborated by the measurable variation of the flange diameters shown in Fig. 6. Measurement of the outer boundary shows a clear transition with a considerable increase in the material flow from the flange. This identifies the draw-in stage, where the process changes from local stretching to global drawing.

Stage 4: Re-strike. The final stage (end of Step 6) shows the sheet completely conformed to the punch. The metal is locked firmly against the punch surface. There is minimal further thinning, while a final increase in pressure, together with the BHF, calibrates the part to ensure dimensional accuracy.

The correspondence between the interrupted steps, punch height, press stroke, and forming stages is summarized in Table 3.

Table 3 Correspondence between interrupted steps, punch height *h*, press stroke *s* (= *h* + 20 mm), and forming stages

Step	Punch height h (mm)	Stroke s (mm)	Forming stage
1	−20	0	Blank inserted; start of pre-bulge
2	0	20	End of pre-bulge (first punch contact)
3	27	47	Thin-out
4	53	73	End of thin-out; onset of draw-in
5	79	99	Draw-in
6	105	125	Draw-in and re-strike

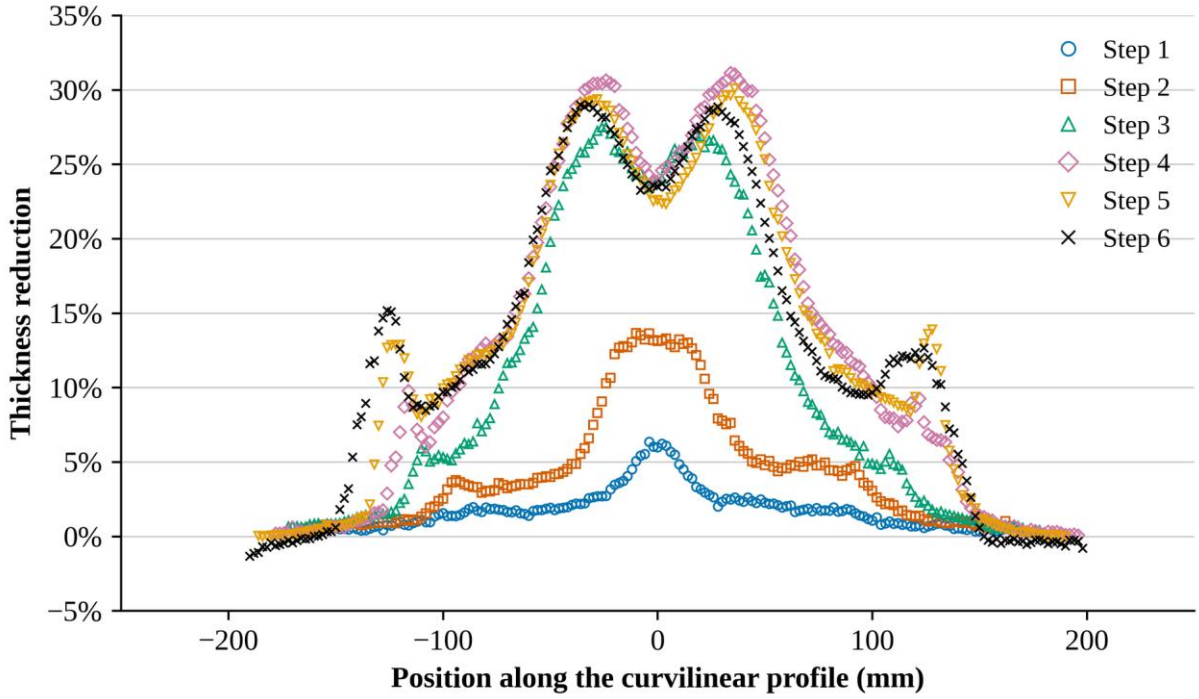


Fig. 5 Distribution of thickness reduction along the curvilinear profile of the cup at different forming steps

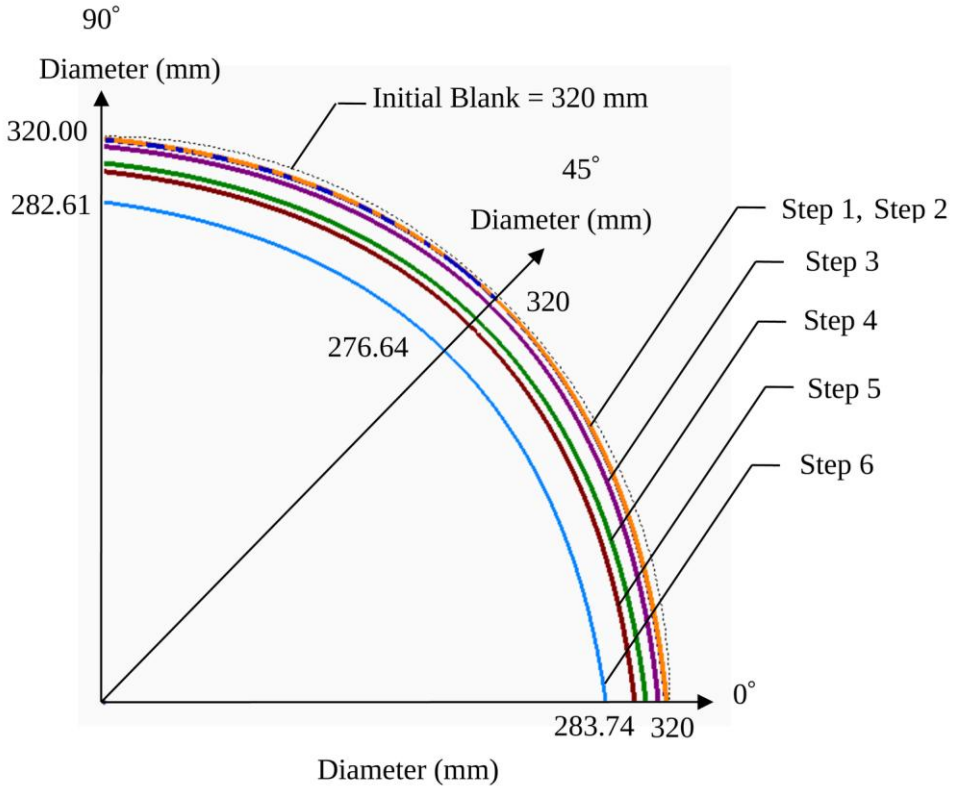
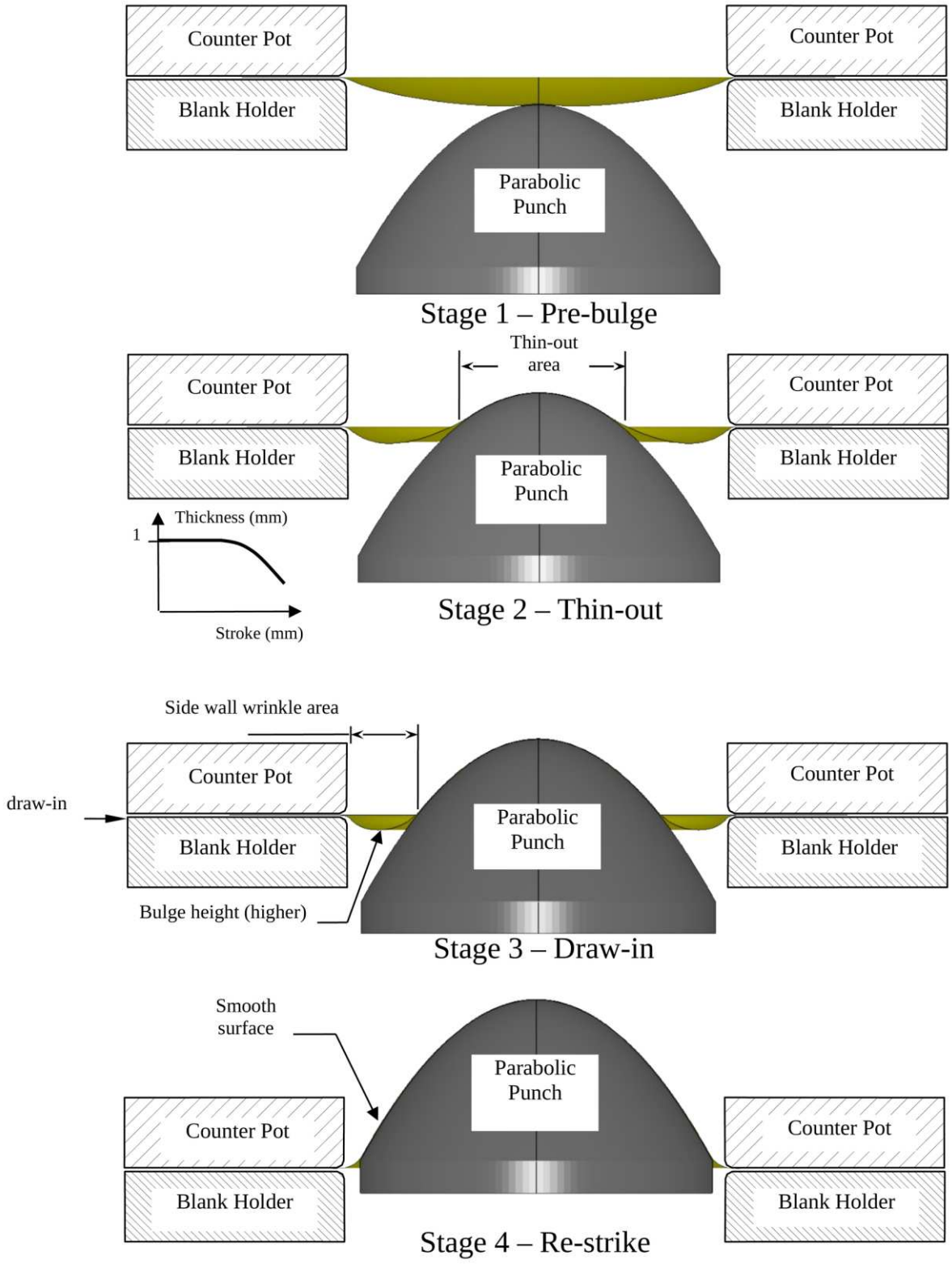


Fig. 6 Flange diameters measured at 0°, 45°, and 90° to the rolling direction at different forming steps

The forming mechanism of a parabolic cup in HMD is shown in Fig. 7. The four stages are pre-bulge, thin-out, draw-in, and re-strike. This model reveals that the severe thinning is not a result of the overall process but is highly localized to the specific mechanics of the thin-out stage.



246

247 **Fig. 7** Four stages of forming a parabolic cup by hydromechanical deep drawing

3.2 Validation of the linear BHF hypothesis

The mechanical insight that the thin-out stage represents the critical window for localized failure led to the hypothesis that reducing the BHF during this stage would facilitate controlled material flow from the flange, thus mitigating excessive stretching and thinning at the punch apex. To test this hypothesis, a linear BHF profile was designed to keep the BHF low during the early to mid-stroke, corresponding directly to the thin-out and early draw-in stages (Fig. 8). This profile differs from the usual constant BHF method, in which a high restraining force is applied throughout the process. The breakpoints of both profiles follow the stage boundaries identified in Sect. 3.1. Up to s = 20 mm (the pre-bulge stage, before punch contact), both profiles apply a low BHF of 100 kN so that the blank can be pre-bulged by the fluid pressure. The pre-bulge condition is therefore identical for both profiles, and any difference in thinning between them originates from the BHF applied after punch contact. The analytical minimum BHF of 203.6 kN in Table 2 refers to the forming stages after punch contact, not to the pre-bulge stage. In the conventional profile, hereafter referred to as the constant BHF because the force is held constant after the pre-bulge stage, the force is then raised to the operating level of 800 kN (Table 2) by s = 47 mm and held constant until the end of the stroke. In the linear profile, the force is instead increased gradually from 100 kN at s = 20 mm to 800 kN at the end of the stroke (s = 125 mm), so that the BHF during the thin-out stage (s = 20–73 mm) remains well below the operating level, while the full operating force is recovered for the re-strike stage.

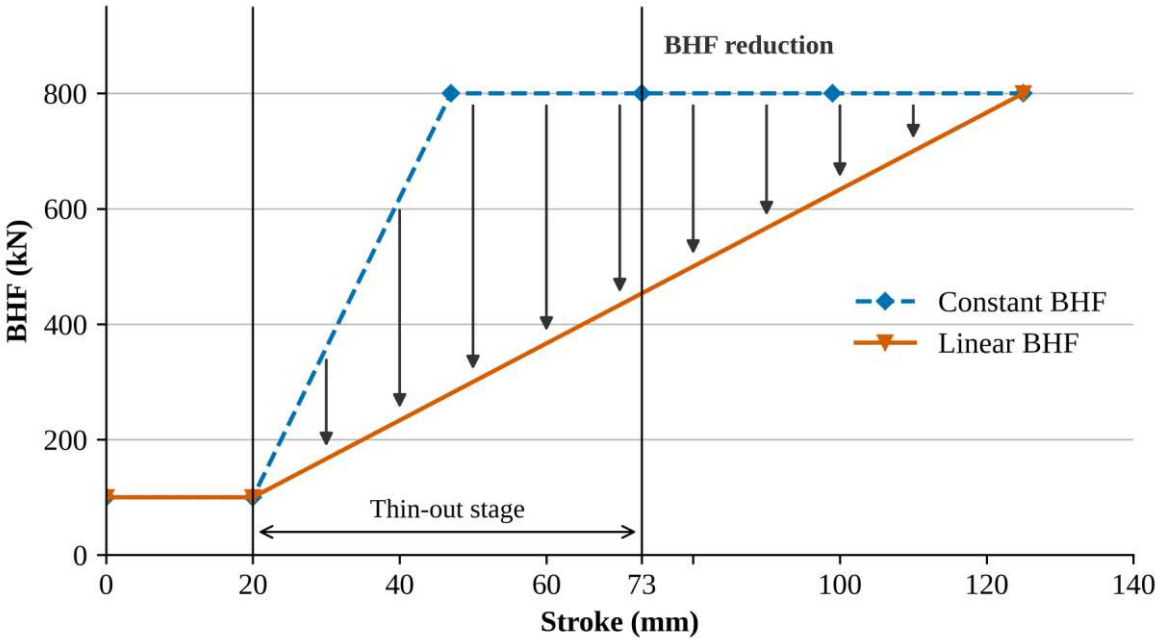
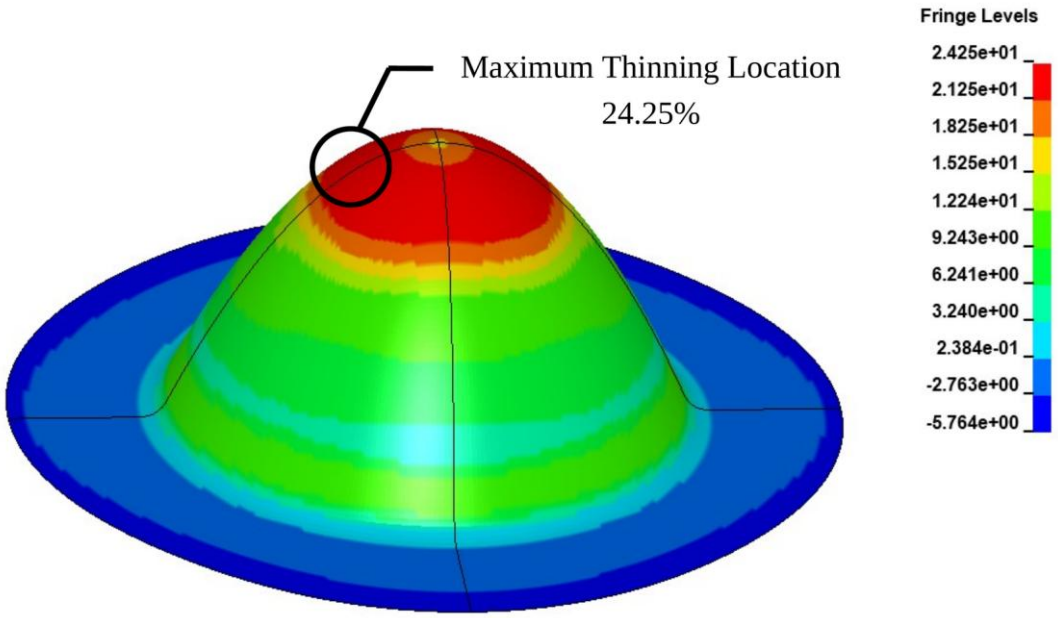


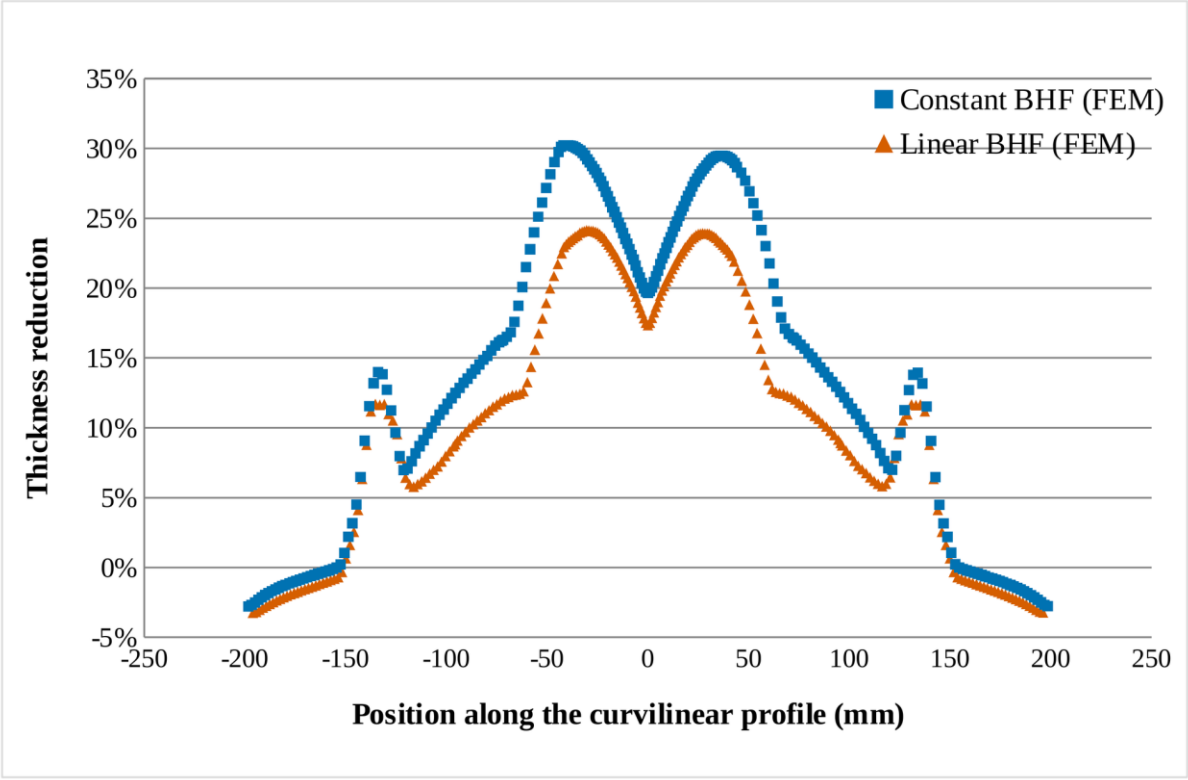
Fig. 8 Constant and linear BHF profiles as functions of punch stroke. The vertical lines at 20 and 73 mm bound the thin-out stage, during which the linear profile keeps the BHF lower. Downward arrows indicate the BHF reduction of the linear profile relative to the constant profile.

The proposed linear BHF strategy was first evaluated with the validated LS-DYNA finite element model. The simulation results strongly supported the hypothesis. As seen in Figs. 9 and 10, the linear BHF profile significantly improved the thickness distribution. The predicted maximum thinning was reduced from 30.33% with a constant BHF to 24.25% with the linear profile. The simulation also showed a more uniform thickness distribution along the cup wall, implying a transition to a more favorable deformation mechanism.



278

279 **Fig. 9** FEM-predicted thinning distribution of a part formed with the linear BHF profile. Fringe
280 levels show the percentage thickness reduction (negative values denote thickening).



281

282 **Fig. 10** FEM-predicted thinning distributions along the curvilinear profile of the cup for the
283 constant and linear BHF profiles

284 The linear BHF strategy was then tested experimentally. As shown in Fig. 11, the maximum
285 measured thinning decreased from 30% with a constant BHF to 25% with the linear profile, in

good agreement with the simulated values. This agreement between the numerical and experimental results validates the accuracy of the finite element model and the practical feasibility of the mechanism-informed loading path.

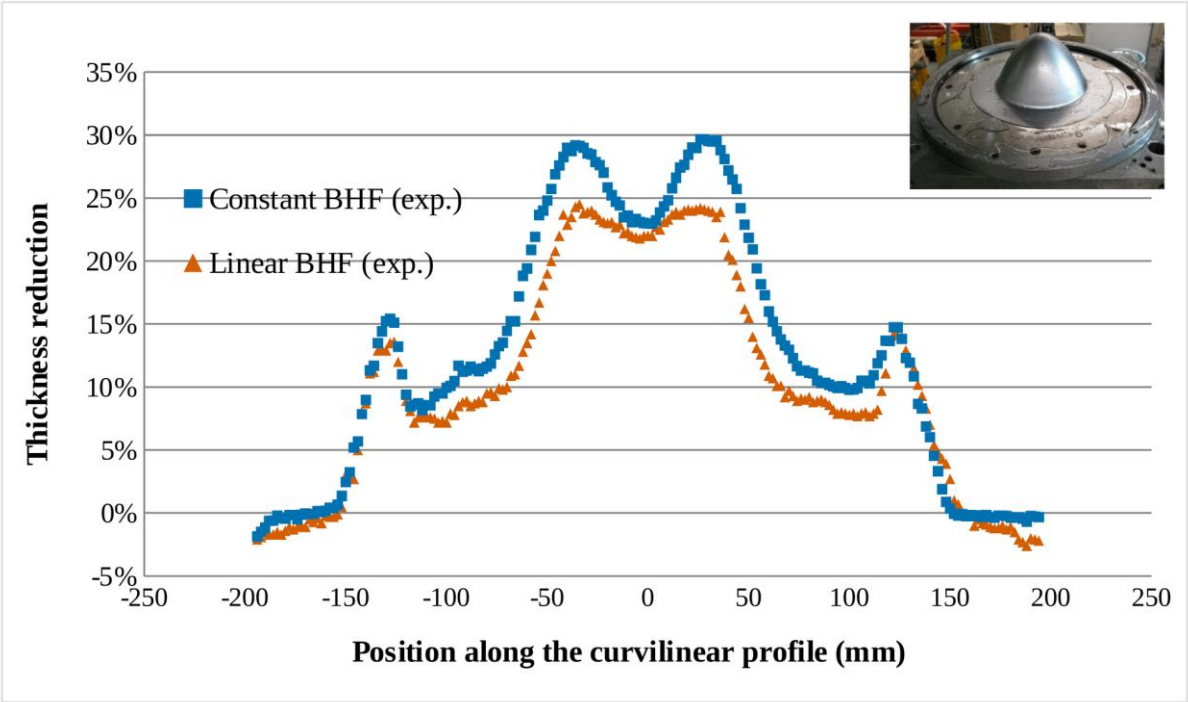


Fig. 11 Experimentally measured thinning distributions along the curvilinear profile of the cup for the constant and linear BHF profiles (inset: image of a formed part)

A key finding of the linear BHF strategy was a significant increase in material flow from the flange. The FE-predicted draw-in at the end of the thin-out stage increased from 6.22 mm (constant BHF) to 9.90 mm (linear BHF), an improvement of 59.1% (Fig. 12a, b). This increase in draw-in indicates that the strategic reduction of the BHF effectively lowers the frictional resistance at the flange, allowing more material to be drawn into the die cavity to feed the forming zone. This result provides direct evidence for the main hypothesis that controlling the BHF during the critical thinning stage can significantly change the material flow behavior.

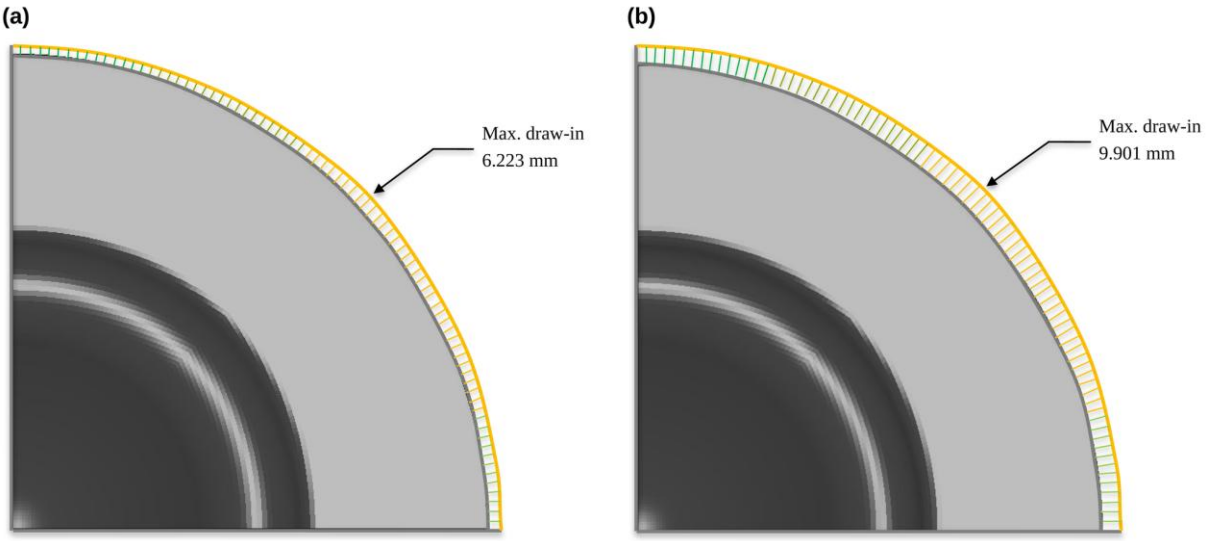


Fig. 12 FE-predicted maximum flange draw-in at the end of the thin-out stage: (a) constant BHF profile (6.223 mm); (b) linear BHF profile (9.901 mm)

3.3 Transition from uniaxial tension to a drawing-dominated mode

To quantitatively confirm the change of deformation mode, a systematic strain analysis was performed, focusing mainly on the critical window of maximum thinning.

3.3.1 Measurement strategy and cluster location

Strain measurement was performed at the 73 mm punch stroke, specifically targeting the "free-forming zone", i.e., the region where the blank is not in direct contact with either the punch or the blank holder, as shown in Fig. 13. This location was selected because it accurately captures the transient response of the material flow to the BHF. Single-element values can be sensitive to local mesh effects, so the strain state was evaluated as the average over a cluster of elements within the critical thinning region of the FE model rather than at a single node. This spatial averaging ensures that the evaluated strain paths represent the macroscopic deformation behavior of the thin-out zone rather than numerical deviations. The 73 mm stroke corresponds to the end of the thin-out stage (punch height 53 mm, Step 4). It is notable that the biaxial tension described for Stage 2 in Sect. 3.1 refers to the apex region at the onset of punch contact, whereas the strain cluster analyzed here lies in the free-forming zone at the end of the thin-out

stage, where the unsupported wall is stretched predominantly in the meridional direction. The two observations therefore describe different regions and instants of the same stage.

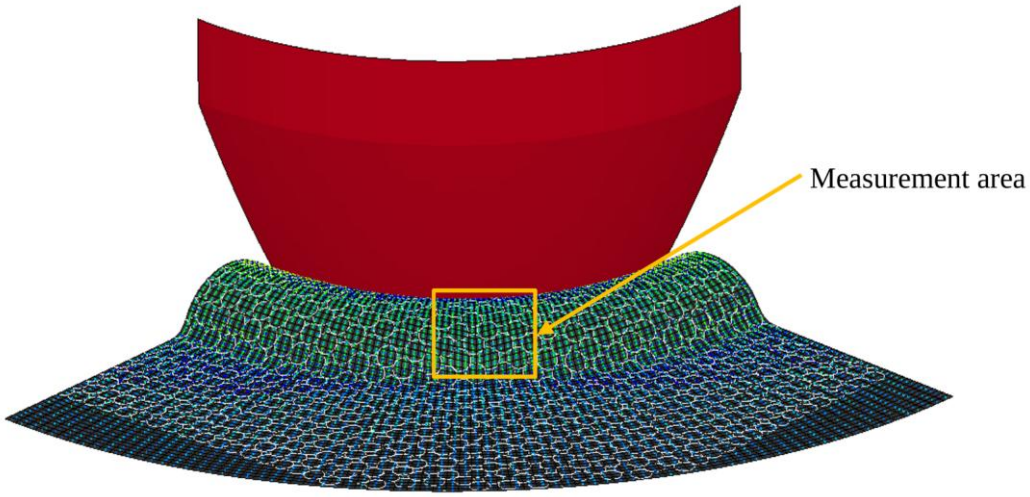


Fig. 13 Location of the element cluster used for strain measurement at a punch stroke of 73 mm (thin-out stage)

3.3.2 FLD deformation mode transformation

The acquired strain cluster was plotted on a forming limit diagram (FLD) to quantitatively evaluate the effect of BHF control on the deformation path of the material (Fig. 14). The forming limit curve (FLC) was constructed using the Keeler-Goodwin model. The analysis shows a sharp change in the mechanical state of the apex region:

- **Constant BHF profile:** For the constant high BHF, the strain cluster lies around a major strain (ε_1) of 8.04% and a minor strain (ε_2) of −4.04%. This corresponds to a strain ratio ($\beta = \varepsilon_2/\varepsilon_1$) of −0.50, which defines a uniaxial tensile mode. Physically, this means that the flange is highly constrained, so, therefore, the material at the apex is pulled longitudinally with little lateral contraction, which increases localized thinning.
- **Linear BHF profile:** The linear BHF profile shifted the cluster further into the drawing quadrant of the FLD. The average major strain increased to 10.55%, while the minor strain became significantly more negative (−7.32%). This resulted in an improved strain ratio (β) of −0.69.

This shift from −0.50 to −0.69 represents a critical transition from uniaxial tension toward a drawing-dominated mode (which approaches pure shear/drawing at $\beta = -1.0$). By reducing the BHF during the thin-out stage, the circumferential constraint is relaxed, allowing the material to undergo greater lateral contraction (more negative minor strain) as it is drawn into the die. This mechanistic shift is the fundamental reason for the 59.1% increase in material draw-in and the resulting preservation of wall thickness at the parabolic apex.

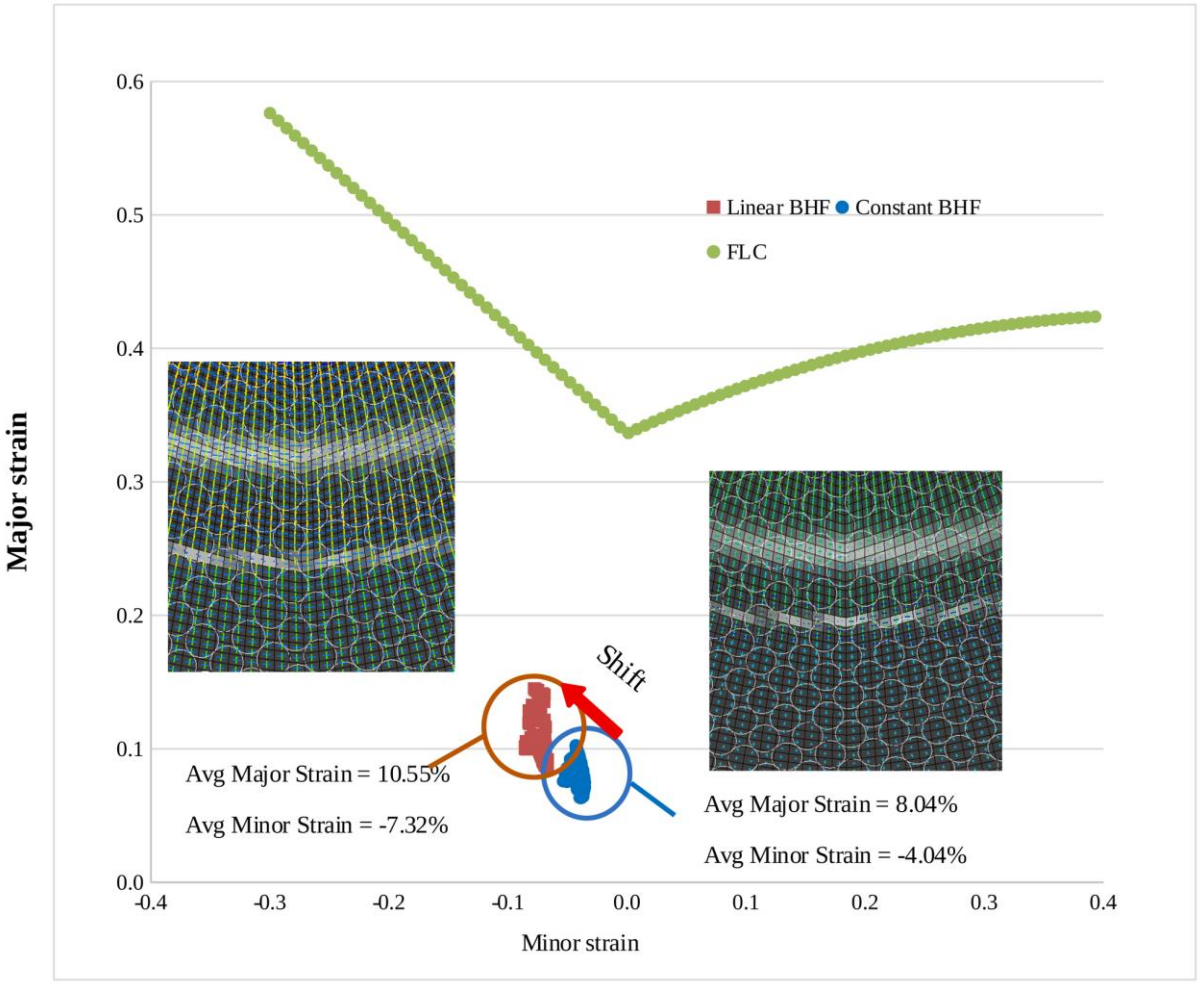


Fig. 14 Forming limit diagram (FLD) at a punch stroke of 73 mm comparing the strain clusters for the constant and linear BHF profiles. The strain state shifts from an ideal uniaxial tensile mode ($\beta = -0.50$, constant BHF) to a drawing-dominated mode ($\beta = -0.69$, linear BHF), allowing greater lateral contraction and material flow while reducing localized thinning at the parabolic apex. Insets show the measured element clusters

3.4 Process limits and bi-linear BHF evolution

While the linear BHF profile significantly improved the thickness distribution, the FLD analysis also revealed a fundamental process limitation: reducing the BHF during the thin-out stage moves the strain path closer to the wrinkling limit, and an excessive reduction introduces a risk of flange wrinkling. To expand the process window, a bi-linear BHF profile is proposed (Fig. 15). Based on the four-stage mechanism, the BHF is decreased during the thin-out stage to prevent fracture and then increased during the draw-in and re-strike stages to suppress wrinkling. The FE simulation in Fig. 16 indicates that this bi-linear strategy further improves part quality, with a predicted maximum thinning of only 23.74%, while no flange wrinkling is predicted by the FE model.

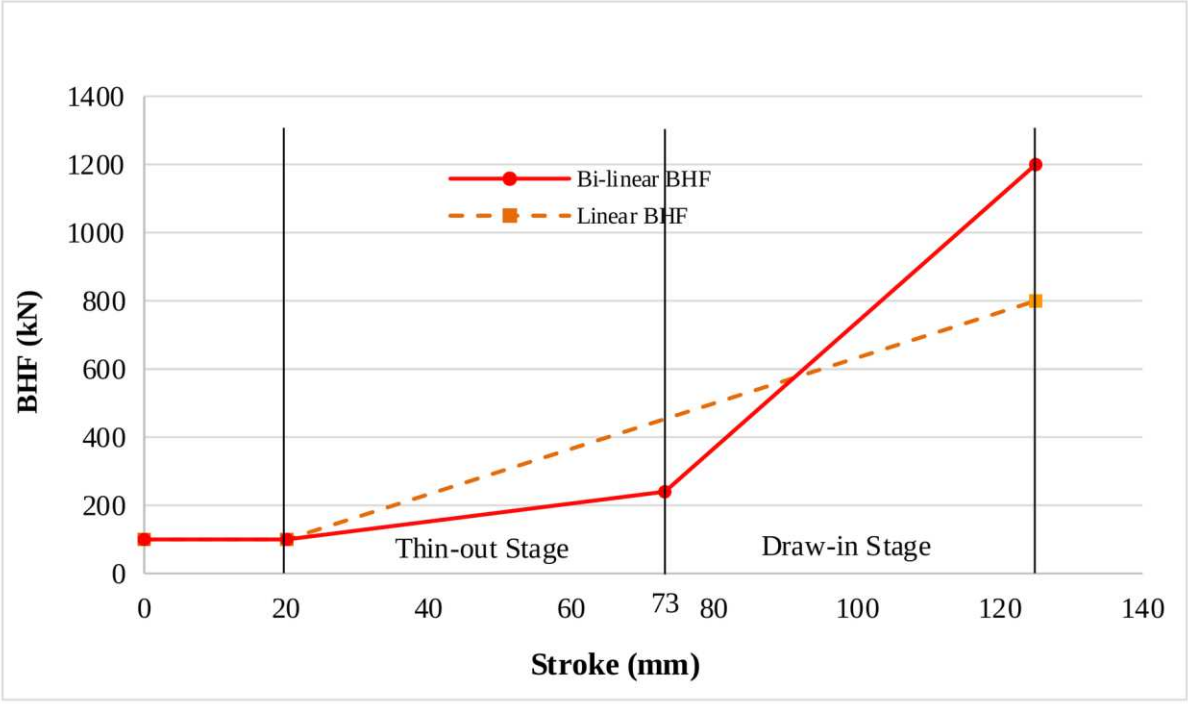


Fig. 15 Proposed bi-linear BHF profile compared with the linear profile: the force is reduced during the thin-out stage to mitigate thinning and then increased during the draw-in and re-strike stages to prevent flange wrinkling

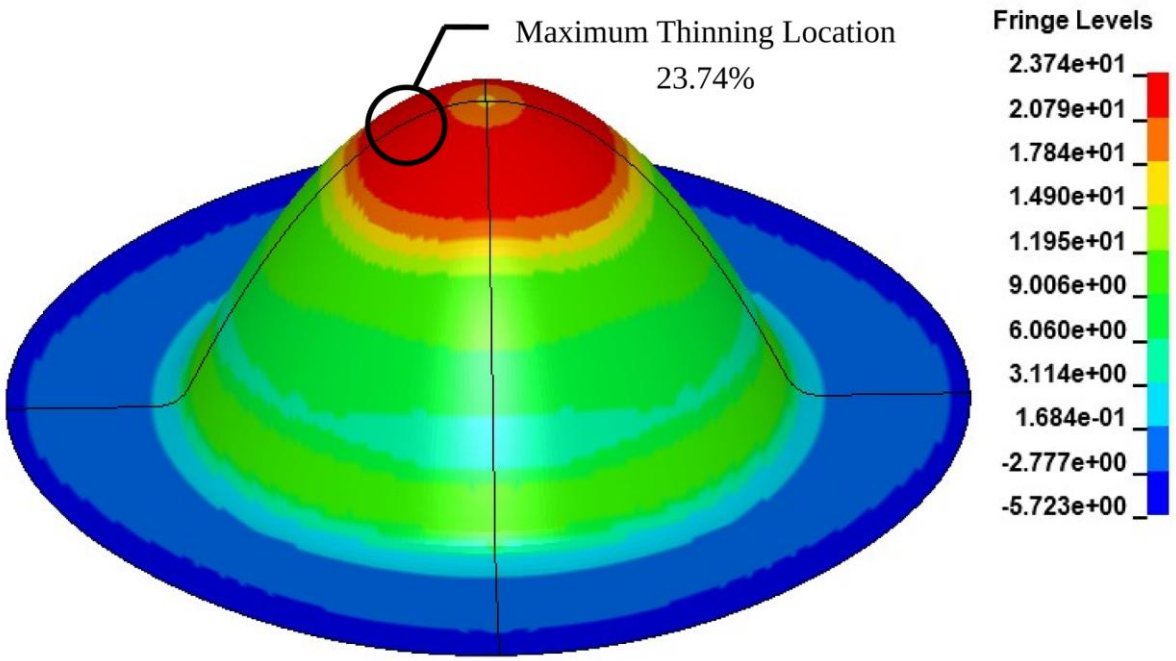


Fig. 16 FEM-predicted thinning distribution of a part formed with the bi-linear BHF profile, showing a maximum thinning of 23.74%. Fringe levels show the percentage thickness reduction (negative values denote thickening)

4 Conclusions

This research proposed a mechanism-based framework for the hydromechanical deep drawing (HMD) of SPCC parabolic cups that goes beyond traditional black-box optimization. It provides an interpretable procedure for designing loading paths in which each segment of the BHF profile is linked to an identified deformation stage. The following conclusions are drawn from the analytical empirical equations, systematic interrupted drawing experiments, and numerical validation.

1. The HMD process for complex parabolic geometries was broken down into four physical stages: pre-bulge, thin-out, draw-in, and re-strike. This provides a clear insight into the transient deformation path, which is often missed by purely numerical studies.
2. Physical measurements of interrupted tests confirmed that the thin-out stage is the critical failure window. The rapid acceleration of thinning upon the first punch contact makes this interval a major constraint on process success.

3. Cluster-averaged FE strains plotted on the FLD provided clear evidence of the mechanistic shift. The optimized BHF scheduling changed the average strain ratio (β) from a uniaxial tensile mode (−0.50) to a drawing-dominated mode (−0.69). This confirms that the material could use its circumferential compression capacity to feed the apex.
4. The linear BHF profile resulted in a 59.1% increase in material draw-in (from 6.223 to 9.901 mm, FE prediction) and a decrease in maximum thinning from 30 to 25%, which directly correlates with the improved strain path observed on the FLD.
5. To expand the process window, a bi-linear BHF profile is proposed. It uses the four-stage approach to decrease the BHF during thin-out and increase it during the subsequent draw-in and re-strike stages. The FE-based evaluation indicates that part quality can be further improved, with a predicted maximum thinning of 23.74%, while no flange wrinkling is predicted.

This study was limited to a single parabolic geometry and one sheet material, and the bi-linear profile was only numerically evaluated. Future work will experimentally validate the bi-linear profile, quantify the wrinkling margin, and assess the transferability of the stage-based procedure to other severely curved axisymmetric geometries and materials.

References

1. Zhang SH, Danckert J (1998) Development of hydro-mechanical deep drawing. J Mater Process Technol 83:14–25. https://doi.org/10.1016/S0924-0136(98)00039-9
2. Bell C, Corney J, Zuelli N, Savings D (2020) A state of the art review of hydroforming technology. Int J Mater Form 13(5):789–828. https://doi.org/10.1007/s12289-019-01507-1
3. Zhang SH, Lang LH, Kang DC, Danckert J, Nielsen KB (2000) Hydromechanical deep-drawing of aluminum parabolic workpieces—experiments and numerical simulation. Int J Mach Tools Manuf 40(10):1479–1492. https://doi.org/10.1016/S0890-6955(00)00006-7

406 4. Liu W, Xu Y, Yuan S (2014) Effect of pre-bulging on wrinkling of curved surface part
407 by hydromechanical deep drawing. Procedia Eng 81:914–920.
408 https://doi.org/10.1016/j.proeng.2014.10.117
409 5. Koç M (2008) Hydroforming for advanced manufacturing. Woodhead Publishing,
410 Cambridge. https://doi.org/10.1533/9781845694418
411 6. Choi H, Koç M, Ni J (2007) Determination of optimal loading profiles in warm
412 hydroforming of lightweight materials. J Mater Process Technol 190(1–3):230–242.
413 https://doi.org/10.1016/j.jmatprotec.2007.02.040
414 7. Öztürk E, Türköz M, Halkaci HS, Koç M (2017) Determination of optimal loading
415 profiles in hydromechanical deep drawing process using integrated adaptive finite
416 element analysis and fuzzy control approach. Int J Adv Manuf Technol 88:2443–2459.
417 https://doi.org/10.1007/s00170-016-8912-x
418 8. Intarakumthornchai T, Jirathearanat S, Thongprasert S, Dechaumphai P (2010) FEA
419 based optimization of blank holder force and pressure for hydromechanical deep
420 drawing of parabolic cup using 2-D interval halving and RSM methods. Eng J
421 14(2):15–32. https://doi.org/10.4186/ej.2010.14.2.15
422 9. Lang LH, Danckert J, Nielsen KB (2004) Investigation into the effect of pre-bulging
423 during hydromechanical deep drawing with uniform pressure onto the blank. Int J Mach
424 Tools Manuf 44(6):649–657. https://doi.org/10.1016/j.ijmachtools.2003.11.004
425 10. Singh SK, Dixit A, Ravi Kumar D (2008) Optimization of the design parameters of
426 modified die in hydro-mechanical deep drawing using LS-DYNA. Int J Adv Manuf
427 Technol 40(1–2):41–46. https://doi.org/10.1007/s00170-008-1383-9
428 11. Obermeyer EJ, Majlessi SA (1998) A review of recent advances in the application of
429 blank-holder force towards improving the forming limits of sheet metal parts. J Mater
430 Process Technol 75(1–3):222–234. https://doi.org/10.1016/S0924-0136(97)00368-3
431 12. Sheng ZQ, Jirathearanat S, Altan T (2004) Adaptive FEM simulation for prediction of
432 variable blank holder force in conical cup drawing. Int J Mach Tools Manuf 44(5):487–
433 494. https://doi.org/10.1016/j.ijmachtools.2003.11.001
434 13. Lin ZQ, Wang WR, Chen GL (2007) A new strategy to optimize variable blank holder
435 force towards improving the forming limits of aluminum sheet metal forming. J Mater
436 Process Technol 183(2–3):339–346. https://doi.org/10.1016/j.jmatprotec.2006.10.027

14. Modi B, Kumar DR (2013) Development of a hydroforming setup for deep drawing of square cups with variable blank holding force technique. Int J Adv Manuf Technol 66(5–8):1159–1169. https://doi.org/10.1007/s00170-012-4397-4

15. Dong C, Ma J, Han H, Zhang W, Liu F, Yang L (2025) Pre-bulging hydromechanical deep-drawing forming performance of a hydraulic punch for stepped parts. J Braz Soc Mech Sci Eng 47:330. https://doi.org/10.1007/s40430-025-05770-z

16. Kimura S, Furushima T (2023) New small-scale hydromechanical deep-drawing process using die-integrated active high-pressure generation system. Int J Mater Form 16:46. https://doi.org/10.1007/s12289-023-01773-0

17. Cai GS, Wu CY, Gao ZP, Lang LH, Alexandrov S (2018) Investigation on the effect of pressure rate on formability of aluminum alloy during warm/hot sheet hydroforming. AIP Adv 8(9):095313. https://doi.org/10.1063/1.5050222

18. Fereshteh-Saniee F, Yaghoubi S (2023) Textural and microstructural analyses and ranking of the process parameters in hydromechanical deep drawing of AZ31B magnesium sheets. J Mater Res Technol 24:9261–9272. https://doi.org/10.1016/j.jmrt.2023.05.126

19. Yaghoubi S, Fereshteh-Saniee F (2023) Effects of process variables on the uniformity of Al-St and Al-Mg laminated composite cups produced by hydro-mechanical deep drawing operation. Proc Inst Mech Eng B J Eng Manuf 237(3):424–434. https://doi.org/10.1177/09544054221102239

20. Shen W, Zhang Z, Zhang W, Zhuang X, Zhao Z (2026) A segmented optimization of time-varying extra hydraulic pressure in hydromechanical deep drawing process for wrinkle reduction. Struct Multidiscip Optim 69:66. https://doi.org/10.1007/s00158-026-04277-y

21. Turkoz M, Cora ON, Gedikli H, Dilmec M, Halkaci HS, Koc M (2020) Numerical optimization of warm hydromechanical deep drawing process parameters and its experimental verification. J Manuf Process 57:344–353. https://doi.org/10.1016/j.jmapro.2020.06.020

Statements and Declarations

Funding No specific grant was received for this research. The hydroforming press and dies used in the experiments were provided by the National Metal and Materials Technology Center (MTEC), National Science and Technology Development Agency (NSTDA), Thailand.

Competing interests The authors have no relevant financial or non-financial interests to disclose.

Author contributions Thanasan Intarakumthornchai conceptualized the study, performed the finite element simulations, prepared the experimental setup and testing equipment, analyzed the experimental data, and drafted the manuscript. Yingyot Aue-u-lan provided academic supervision and verified the methodology. All authors read and approved the final manuscript.

Ethics approval Not applicable. This study did not involve human participants or animals.

Consent to participate Not applicable.

Consent for publication Not applicable.

Data availability The data that support the findings of this study are available from the corresponding author upon reasonable request.

Code availability Not applicable.